



Spatial Kramers-Kronig relation and unidirectional light reflection induced by Rydberg interactionsDi-Di Zheng , Yan Zhang , Yi-Mou Liu, Xiao-Jun Zhang,^{*} and Jin-Hui Wu[†]*School of Physics and Center for Quantum Sciences, Northeast Normal University, Changchun 130024, China*

(Received 20 April 2022; accepted 16 December 2022; published 5 January 2023)

Kramers-Kronig (KK) relation between the dispersion and absorption responses of a signal field can be mapped from the frequency domain into the space domain via the dipole-dipole interactions between a sample of homogeneous target atoms and a ring of equally spaced control atoms. This is achieved by establishing an effective two-level configuration for the target atoms in the far-detuned driving regime of both lower and upper transitions while maintaining the maximal Rydberg excitations for the control atoms via an antiblockade driving scheme of the lower and upper transitions. We find, in particular, that it is viable to realize a tunable spatial KK relation supporting asymmetric and even unidirectional reflection for appropriate signal frequencies in a desired range depending on the frequency of a coupling field. Taking a periodic lattice of target atoms instead, the multiple Bragg scattering can be incorporated into the spatial KK relation in order to enhance the nonzero reflectivity yet without breaking the asymmetric or unidirectional reflection.

DOI: [10.1103/PhysRevA.107.013704](https://doi.org/10.1103/PhysRevA.107.013704)**I. INTRODUCTION**

In recent years, great efforts have been made in the realization and manipulation of asymmetric light reflection and even unidirectional invisibility with artificial optical structures of complex optical potentials [1–24]. One main motivation lies in that relevant advances are essential for developing one-way optical devices unattainable with natural linear materials of real optical potentials. Reflection and transmission properties are typically bidirectional and symmetric for isotropic linear materials based on the Lorentz reciprocal theorem [25,26]. This can also be understood in view of information optics, which argues that the Fourier transform of a real optical potential is definitely symmetric so that light propagation in natural linear materials always results in balanced forward and backward modes [27,28].

Now it is known that unidirectional reflection and invisibility can be attained at an exceptional point in non-Hermitian media exhibiting, e.g., parity-time (\mathcal{PT}) symmetry [1–13]. These media are, however, very challenging with regard to the experimental implementation because they require elaborate designs of gain and loss. Horsley *et al.* found in 2015 that electromagnetic waves incident upon an inhomogeneous medium, the real and imaginary parts of whose complex permittivity are related in space via the Kramers-Kronig (KK) relation, can be efficiently absorbed from one side but are normally reflected from the other side [14]. Soon afterwards, results in this pioneer work were extended in theory [15–20], verified in experiment [21–23], and explored to develop new techniques of holographic imaging or anechoic chamber [29–31]. Such spatial KK media, though requiring no elaborate designs on gain and loss, are typically designed with fixed structures

and lack the dynamic tunability. A feasible method for overcoming this difficulty is to consider multilevel driven atomic systems, in which the frequency-to-space mapping of an induced susceptibility can be attained via a dynamic Stark or Zeeman effect [24].

On the other hand, we note that nonlocal dipole-dipole interactions (DDIs) of Rydberg atoms depend critically on the interatomic distance R and can be manipulated on demand by external driving fields [32–35]. This then motivates us to seek a feasible driving scheme where DDIs can be used to realize the spatial KK relation by establishing a nonlinear dependence of atomic transition frequency on atomic spatial position. To be more specific, DDIs may manifest as either van der Waals (vdW) potentials scaling as $1/R^6$ in the nonresonant regime or Förster-like potentials scaling as $1/R^3$ in the resonant regime [36]. In fact, Rydberg atoms have been well studied as an intriguing platform for realizing quantum information processing [37–41] and high-precision field sensing [42–46], considering that they also exhibit the features of long radiative lifetimes and large electric dipole moments. Note also that Rydberg atoms have been explored in the regime of electromagnetically induced transparency to achieve effective interactions between individual photons, which promise the realization of nontrivial photonic devices like single-photon sources [47–49], memorizers [50–52], and transistors [53–55]. To the best of our knowledge, DDIs of Rydberg atoms have not been considered to develop photonic devices supporting asymmetric light propagation.

We examine here an effective scheme for the realization of a tunable spatial KK relation in a sample of vast homogeneous target atoms by utilizing their vdW interactions with a ring of six equally spaced control atoms. This has been done by considering an antiblockade driving configuration for the control atoms in the dark-state [56,57] regime while considering a far-detuned driving configuration for the target atoms in the EIT regime. Under appropriate conditions, the control atoms can

^{*}zhangxj037@nenu.edu.cn[†]jhwu@nenu.edu.cn

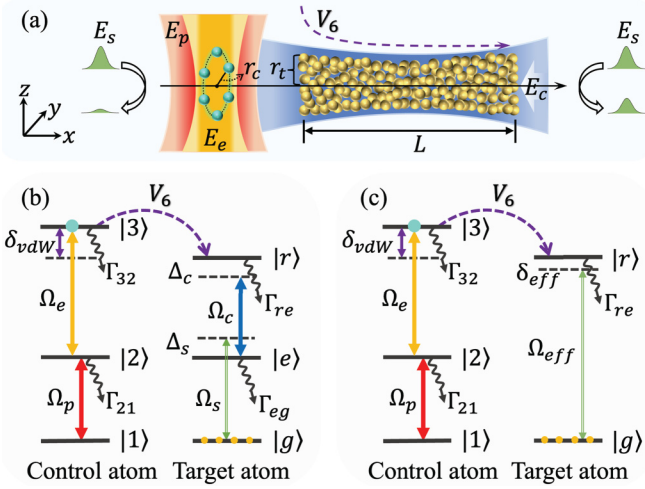


FIG. 1. (a) Schematic of asymmetric reflection of a signal (E_s) field incident upon a cylindrical sample of target atoms with length L and radius r_t in the presence of a coupling (E_c) field. Six control atoms arranged in a ring with radius r_c are irradiated by a pumping (E_p) and an exciting (E_e) field to manipulate all target atoms via vdW (\mathcal{V}_6) interactions. (b) Driving energy-level configurations for a pair of control and target atoms interacting via the \mathcal{V}_6 potential. The pumping (Ω_p) and exciting (Ω_e) fields are applied on the control atom in a resonant way to realize the excitation of the Rydberg state $|3\rangle$. The signal (Ω_s) and coupling (Ω_c) fields are applied on the target atom in an off-resonance way to avoid the excitation of the intermediate state $|e\rangle$. (c) Effective energy-level configurations for a pair of control and target atoms when the intermediate state $|e\rangle$ is eliminated and the signal and coupling fields are replaced by an effective (Ω_{eff}) field under appropriate conditions.

be made to exhibit roughly maximal Rydberg excitations via a dark-state manipulation while the target atoms may reduce from a three-level to a two-level configuration by adiabatically eliminating the intermediate state. On this account, it is viable to realize a nonlinear frequency-to-space mapping of the dispersion and absorption responses and hence a well-established and modulated spatial KK relation. Consequently, the reflectivity of a signal field incident upon one side is distinct from that upon the other side and may even become vanishing to result in unidirectional reflection. Replacing the homogeneous atomic sample with a periodic atomic lattice, it is viable to further improve the asymmetric and unidirectional reflection behaviors, e.g., by enhancing the nonzero reflectivity yet without activating the vanishing reflectivity, when multiple Bragg scattering is incorporated into a spatial KK relation.

II. MODEL AND EQUATIONS

We start by introducing our basic model in Fig. 1(a), where a signal field of amplitude (frequency) E_s (ω_s) is incident upon a cylindrical sample of homogeneous target atoms with radius r_t in the yz plane and length L along the x direction. The overall optical response of target atoms with density N_0 is modulated via the vdW interactions arising from six equally spaced control atoms arranged as a ring with radius r_c in the yz plane at $x = x_0$. These control atoms at positions (x_0, \vec{r}_k) can generate a distance-dependent vdW potential upon a target

atom at position (x, \vec{r}) ,

$$\mathcal{V}_6 = \sum_{k=1}^6 \frac{C_6}{[(x - x_0)^2 + |\vec{r} - \vec{r}_k|^2]^3}, \quad (1)$$

with coefficient C_6 . This vdW potential can be assumed, to a good approximation, to be transversely homogeneous as a mean result of six control atoms and hence depends only on the longitudinal coordinate x (cf. the first paragraph of Sec. III). Note also that two-dimensional Gaussian traps have been considered to restrict motions of the control and target atoms in both x and y directions. Each control atom is driven by a pumping field of amplitude (frequency) E_p (ω_p) on transition $|1\rangle \leftrightarrow |2\rangle$ and an exciting field of amplitude (frequency) E_e (ω_e) on transition $|2\rangle \leftrightarrow |3\rangle$ as shown in Fig. 1(b), with $\Omega_p = E_p \wp_{21} / 2\hbar$ and $\Omega_e = E_e \wp_{32} / 2\hbar$ being the Rabi frequencies while $\Delta_p = \omega_p - \omega_{21}$ and $\Delta_e = \omega_e - \omega_{32}$ being the detunings. Each target atom is driven by the signal field on transition $|g\rangle \leftrightarrow |e\rangle$ and a coupling field of amplitude (frequency) E_c (ω_c) on transition $|e\rangle \leftrightarrow |r\rangle$ as shown in Fig. 1(b), with $\Omega_s = E_s \wp_{eg} / 2\hbar$ and $\Omega_c = E_c \wp_{re} / 2\hbar$ being the Rabi frequencies while $\Delta_s = \omega_s - \omega_{eg}$ and $\Delta_c = \omega_c - \omega_{re}$ being the detunings. We have used $\wp_{\mu\nu}$ and $\omega_{\mu\nu}$ to denote dipole moments and resonant frequencies, respectively, on transitions $|\mu\rangle \leftrightarrow |\nu\rangle$ with $\{\nu, \mu\} \in \{1, 2, 3\}$ for control atoms while $\{\nu, \mu\} \in \{g, e, r\}$ for target atoms.

To be more specific, here we take ground states $|1\rangle \equiv |5S_{1/2}, F = 1\rangle$ and $|g\rangle \equiv |5S_{1/2}, F = 2\rangle$, intermediate states $|2\rangle \equiv |5P_{3/2}, F = 0\rangle$ and $|e\rangle \equiv |5P_{3/2}, F = 3\rangle$, and Rydberg states $|3\rangle = |r\rangle \equiv |60S_{1/2}\rangle$ for the ^{87}Rb isotope as an example. In this case, the signal and coupling fields have negligible effects on, albeit traveling through, the control atoms because they remain far detuned from the $|1\rangle \leftrightarrow |2\rangle$ and $|2\rangle \leftrightarrow |3\rangle$ transitions, respectively. The pumping and exciting fields, however, do not travel through the target atoms as arranged in Fig. 1(a) and are assumed to be applied before the signal and coupling fields. We further consider that the control atoms will be driven in an antiblockade way to exhibit maximal Rydberg populations while the target atoms will be driven in the weak signal limit to exhibit negligible Rydberg populations. Then it is viable to neglect the Rydberg interactions between target atoms as well as the retroaction of target atoms on control atoms (cf. the second paragraph of Sec. III) so that we can write down the following Hamiltonians:

$$\begin{aligned} H_c / \hbar &= -\Delta_p \sigma_{22} - (\Delta_p + \Delta_e + \delta_{vdW}) \sigma_{33} \\ &\quad - \Omega_p \sigma_{21} - \Omega_e \sigma_{32} - \Omega_p^* \sigma_{12} - \Omega_e^* \sigma_{23}, \\ H_t / \hbar &= -\Delta_s \sigma_{ee} - (\Delta_s + \Delta_c) \sigma_{rr} - \Omega_s \sigma_{eg} - \Omega_c \sigma_{re} \\ &\quad - \Omega_s^* \sigma_{ge} - \Omega_c^* \sigma_{er} + \mathcal{V}_6 \sigma_{33} \sigma_{rr}, \end{aligned} \quad (2)$$

for the control and target atoms in order. Here we have introduced $\sigma_{\nu\mu} = |\nu\rangle\langle\mu|$ to denote the transition ($\nu \neq \mu$) or projection ($\nu = \mu$) operator and δ_{vdW} to denote the mean shift of a control atom arising from its vdW interactions with other control atoms. The scheme described by Eq. (2) is expected to work also for a quantized single-photon signal field, with which it is natural to neglect the vdW interactions between target atoms as well as the retroaction of target atoms on control atoms.

Dynamic evolutions of control atoms are governed by the master equation for the density operator ρ :

$$\partial_t \rho = -i[H_c/\hbar, \rho] + \mathcal{L}_c(\rho), \quad (3)$$

where $\mathcal{L}_c(\rho) = \sum \Gamma_{\mu\nu}[\sigma_{\nu\mu}\rho\sigma_{\mu\nu} - \frac{1}{2}(\rho\sigma_{\mu\nu}\sigma_{\nu\mu} + \sigma_{\mu\nu}\sigma_{\nu\mu}\rho)]$ describes the dissipation processes contributed by population decay rates Γ_{32} and Γ_{21} on the $|3\rangle \leftrightarrow |2\rangle$ and $|2\rangle \leftrightarrow |1\rangle$ transitions, respectively. Using H_c and $\mathcal{L}_c(\rho)$, it is easy to expand Eq. (3) into a set of dynamic equations on nine density matrix elements $\rho_{\mu\nu}$ with $\{\mu, \nu\} \in \{1, 2, 3\}$. These equations can be solved by setting $\partial_t \rho_{\mu\nu} = 0$ to attain the steady-state [56,57] Rydberg population,

$$\rho_{33} \simeq \frac{(\gamma_{21} + \gamma_{31})\Omega_p^2\Omega_e^2}{\gamma_{21}\Omega_e^4 + (\gamma_{21} + 3\gamma_{31})\Omega_p^2\Omega_e^2 + \gamma_{21}^2\gamma_{31}\Omega_e^2}, \quad (4)$$

in the antiblockade driving limit of $\Delta_p = \Delta_e + \delta_{\text{vdW}} = 0$ and $\Omega_p \geq \Omega_e > \gamma_{21} \gg \gamma_{31}$ with $\gamma_{31} = \Gamma_{32}/2 + \gamma_{31}^d$ and $\gamma_{21} = \Gamma_{21}/2$. Here γ_{31}^d denotes a pure dephasing rate arising from the finite laser linewidths and has to be included because Γ_{32} is negligible for Rydberg states of high principal quantum numbers. Moreover, γ_{31} should be much smaller than other parameters so as to maintain the dark state $|D\rangle = c_1|1\rangle - c_3|3\rangle$ by excluding the intermediate state $|2\rangle$; hence, it is viable to attain $\rho_{33} = |c_3|^2 \simeq \Omega_p^2/(\Omega_p^2 + \Omega_e^2) \rightarrow 1$ of our interest by further requiring $\Omega_p^2 \gg \Omega_e^2$.

With the same strategy, after introducing population decay rates Γ_{re} and Γ_{eg} as well as dephasing rates $\gamma_{re} = (\Gamma_{re} + \Gamma_{eg})/2$, $\gamma_{rg} = \Gamma_{re}/2 + \gamma_{rg}^d$, and $\gamma_{eg} = \Gamma_{eg}/2$, we can write down a new set of dynamic equations on nine density matrix elements $\rho_{\mu\nu}$ with $\{\mu, \nu\} \in \{g, e, r\}$ for the target atoms. These equations can be solved by setting $\partial_t \rho_{\mu\nu} = 0$ and $\rho_{ee} \rightarrow 0$ in the limits of $\Delta_s \simeq -\Delta_c$, $|\Delta_s| \gg \gamma_{eg} \gg \Omega_s$, and $|\Delta_c| \gg \Omega_c \gg \gamma_{re}$ to attain

$$\begin{aligned} \rho_{rr} &= \frac{2\gamma_{rg}\Omega_{\text{eff}}^2}{\Gamma_{re}[\gamma_{rg}^2 + (\delta_{\text{eff}} + \mathcal{V}_6\rho_{33})^2] + 4\gamma_{rg}\Omega_{\text{eff}}^2}, \\ \rho_{rg} &= \frac{i\Omega_{\text{eff}}\Gamma_{re}[\gamma_{rg} + i(\delta_{\text{eff}} + \mathcal{V}_6\rho_{33})]}{\Gamma_{re}[\gamma_{rg}^2 + (\delta_{\text{eff}} + \mathcal{V}_6\rho_{33})^2] + 4\gamma_{rg}\Omega_{\text{eff}}^2}, \end{aligned} \quad (5)$$

restricted by $\rho_{eg} = -(\Omega_c^*\rho_{rg} + \Omega_s\rho_{gg})/\Delta_s$, $\rho_{re} = (\Omega_s^*\rho_{rg} + \Omega_c\rho_{rr})/\Delta_c$, and $\rho_{gg} + \rho_{rr} = 1$. Here $\Omega_{\text{eff}} = \Omega_s\Omega_c/\Delta_c$ is an effective two-photon Rabi frequency while $\delta_{\text{eff}} = \Delta_s + \Delta_c - \Delta_{e1} - \Delta_{e2}$ is an effective two-photon detuning modified by $\Delta_{e1} = \Omega_c^2/\Delta_s$ and $\Delta_{e2} = \Omega_s^2/\Delta_c$.

Further considering $\gamma_{rg}\Gamma_{re} \gg 4\Omega_{\text{eff}}^2$, which is available by enhancing γ_{rg} with finite laser linewidths [58] and Γ_{re} via incoherent (downward) pumpings [59], we can attain with Eq. (5) an induced signal susceptibility,

$$\chi_s = \frac{N_0\delta_{ge}^2}{\hbar\epsilon_0} \left[\frac{\Omega_c^2}{\Delta_s\Delta_c} \frac{\delta_{\text{eff}} + \mathcal{V}_6\rho_{33} - i\gamma_{rg}}{\gamma_{rg}^2 + (\delta_{\text{eff}} + \mathcal{V}_6\rho_{33})^2} - \frac{1}{\Delta_s} \right], \quad (6)$$

describing the target atoms reduced to a two-level configuration as shown in Fig. 1(c). It is worth noting that χ_s is position dependent in the presence of a vdW potential \mathcal{V}_6 and valid only in the case of $|\delta_{\text{eff}}| \ll |\Delta_s \simeq -\Delta_c|$. We also note that the real (χ'_s) and imaginary (χ''_s) parts of χ_s describe, respectively, the dispersion and absorption responses and are connected via the KK relation in the frequency domain based

on the causality principle and Cauchy's theorem in the case of $\mathcal{V}_6 = 0$ [60].

The KK relation may also hold in the space domain in the case of $\mathcal{V}_6 \neq 0$ for appropriate values of δ_{eff} . This is true only if χ'_s and χ''_s are related through

$$\begin{aligned} \chi''_s(x) &= \frac{1}{\pi} \text{P} \int_0^L \frac{\chi'_s(\xi)}{\xi - x} d\xi, \\ \chi'_s(x) &= \frac{1}{\pi} \text{P} \int_0^L \frac{\chi''_s(\xi)}{x - \xi} d\xi, \end{aligned} \quad (7)$$

where P denotes a Cauchy's principle-value integral with respect to the atomic position ξ . Equation (7) indicates that χ'_s and χ''_s must be spatially out of phase in the case of a perfect spatial KK relation such that the target atoms become unidirectional reflectionless to the signal field [14]. This can be understood by considering that, if χ'_s and χ''_s are spatially out of phase and meanwhile analytical in the upper-half complex plane, their Fourier components will contain only positive wave vectors and hence give rise to no backscattering relevant to negative wave vectors. The degree to which the spatial KK relation is violated can be evaluated by two figures of merit defined, respectively, as

$$\begin{aligned} D_{\text{kk}}^I &= \frac{\int_0^L [|\chi''_s(x)| - |\frac{1}{\pi} \text{P} \int_0^L \frac{\chi'_s(\xi)}{\xi - x} d\xi|] dx}{\int_0^L |\chi''_s(x)| dx}, \\ D_{\text{kk}}^R &= \frac{\int_0^L [|\chi'_s(x)| - |\frac{1}{\pi} \text{P} \int_0^L \frac{\chi''_s(\xi)}{x - \xi} d\xi|] dx}{\int_0^L |\chi'_s(x)| dx}, \end{aligned} \quad (8)$$

with $D_{\text{kk}}^{I,R} \rightarrow 0$ referring to a perfect spatial KK relation in the unbroken regime while a larger $|D_{\text{kk}}^{I,R}|$ indicating a greater degree of violation in the broken regime.

To examine the reflection and transmission spectra, we can resort to the standard transfer matrix method [61] sketched below. First, we partition the cylindrical sample of target atoms into a large number ($J \gg 1$) of thin slices in the x direction labeled by $j \in \{1, J\}$, which exhibit an identical thickness $\ell = L/J$ but different susceptibilities $\chi_s(x) \rightarrow \chi_s(j\ell)$. Second, we establish a 2×2 unimodular transfer matrix $M_j(\ell)$ with its four elements determined by the wave vector $k_s(j\ell) = 2\pi n_s(j\ell)/\lambda_s$ and the refractive index $n_s(j\ell) = \sqrt{1 + \chi_s(j\ell)}$ (see more details in Ref. [61]). This matrix describes the phase and amplitude changes, owing to reflection and transmission, of two signal fields passing through the j th slice from the left and the right side, respectively. To be more specific, $M_j(\ell)$ relates $E_s^+(j\ell - \ell)$ and $E_s^-(j\ell - \ell)$ to $E_s^+(j\ell)$ and $E_s^-(j\ell)$ via

$$\begin{bmatrix} E_s^+(j\ell) \\ E_s^-(j\ell) \end{bmatrix} = M_j(\ell) \begin{bmatrix} E_s^+(j\ell - \ell) \\ E_s^-(j\ell - \ell) \end{bmatrix}, \quad (9)$$

where “+” (“-”) denotes the forward (backward) component of a reflected or transmitted signal field. Third, we attain the total transfer matrix $M(L) = M_J(\ell) \cdots M_j(\ell) \cdots M_1(\ell)$ as a sequential multiplication of the individual transfer matrices of all J slices, which relates $E_s^+(0)$ and $E_s^-(0)$ to $E_s^+(L)$ and $E_s^-(L)$ instead via

$$\begin{bmatrix} E_s^+(L) \\ E_s^-(L) \end{bmatrix} = M(L) \begin{bmatrix} E_s^+(0) \\ E_s^-(0) \end{bmatrix}. \quad (10)$$

Finally, we can rewrite Eq. (10) into another form where the input fields $E_s^+(0)$ and $E_s^-(L)$ are related to the output fields $E_s^+(L)$ and $E_s^-(0)$. In this case, it is straightforward to attain the (asymmetric) reflectivities $R_l \neq R_r$ and the (reciprocal) transmissivities $T = T_{l,r}$ in terms of relevant matrix elements $M_{(ij)}(L)$ restricted by the unimodular requirement $M_{(11)}M_{(22)} - M_{(12)}M_{(21)} = 1$:

$$\begin{aligned} R_l &= \left| \frac{E_s^-(0)}{E_s^+(0)} \right|^2 = \left| \frac{M_{(21)}(L)}{M_{(22)}(L)} \right|^2, \\ R_r &= \left| \frac{E_s^+(L)}{E_s^-(L)} \right|^2 = \left| \frac{M_{(12)}(L)}{M_{(22)}(L)} \right|^2, \\ T &= \left| \frac{E_s^+(L)}{E_s^+(0)} \right|^2 = \left| \frac{E_s^-(0)}{E_s^-(L)} \right|^2 = \left| \frac{1}{M_{(22)}(L)} \right|^2, \end{aligned} \quad (11)$$

where “l” and “r” refer to a signal field incident from the left ($x = 0$) and the right ($x = L$) side, respectively.

So far we have been considering a homogeneous sample of cold target atoms. Now we switch to another scenario where target atoms are trapped in an optical lattice of period Λ and exhibit a periodic Gaussian density:

$$N(x) = \sum_{k=1}^K N_k(x) = \sum_{k=1}^K \frac{\Lambda N_0}{\delta x \sqrt{\pi}} e^{-(x-x_k)^2/\delta x^2}. \quad (12)$$

Here $x_k = (k - 1/2)\Lambda$ denotes the k th unit cell’s center while δx and $\Lambda N_0/\delta x \sqrt{\pi}$ are the common width and peak of all unit cells, respectively. This atomic lattice of mean density N_0 and length $L = K\Lambda$ is examined to show how a nonzero reflectivity is enhanced by incorporating multiple Bragg scattering into a spatial KK relation.

III. RESULTS AND DISCUSSION

We now begin to examine the out-of-phase spatial distributions of χ'_s and χ''_s as well as the asymmetric spectra of R_l and R_r with formulas developed in the last section. To this end, we first specify realistic parameters for the states of ^{87}Rb isotopes mentioned before Eq. (2) with $\Gamma_{32}/2\pi = 0.6$ kHz, $\Gamma_{re}/2\pi = 10$ kHz, $\Gamma_{21,eg}/2\pi = 6.0$ MHz, $\gamma_{31,rg}^d/2\pi = 10$ kHz, $\delta_{eg} = 2.54 \times 10^{-29}$ C m, and $C_6/2\pi = 140$ GHz μm^6 [62–64]. With respect to the applied fields, we choose $\Omega_p/2\pi = 50$ MHz, $\Omega_e/2\pi = 5.0$ MHz, $\Delta_p = 0$, and $\Delta_e = -\delta_{\text{vdW}}$ to achieve the maximal Rydberg population ($\rho_{33} \rightarrow 1$) for all control atoms, while consider $\Omega_s/2\pi = 4$ kHz, $\Omega_c/2\pi = 10$ MHz, and $-\Delta_s/2\pi \simeq \Delta_c/2\pi = 200$ MHz to justify the two-level approximation ($\Omega_{\text{eff}}/2\pi = 0.2$ kHz, $\Delta_{e1}/2\pi = -0.5$ MHz, $\Delta_{e2} \rightarrow 0$) for all target atoms. Taking $r_c = r_t = 3.5 \mu\text{m}$ and $x_0 = -5 \mu\text{m}$, we further have $\rho_{rr}^{\text{max}} \simeq 0.0005$ for the target atoms and $\delta_{\text{vdW}} \simeq 150$ MHz for the control atoms. Moreover, it is appropriate to take $\mathcal{V}_6(x, 0)$ along the central axis with $x \in [0, L]$ and $L = 10 \mu\text{m}$ into the following calculations because the deviation of $\mathcal{V}_6(x, \vec{r})$ [cf. Eq. (1)] in the cylindrical sample of target atoms from a transversely homogeneous potential is less than $\sim 6\%$ when six equally spaced control atoms are arranged in a ring as in Fig. 1(a).

Then, we argue that the Rydberg interactions of target atoms are negligible with density $N_0 = 2.0 \times 10^{12} \text{ cm}^{-3}$ and mean interatomic distance $d = (1/N_0)^{1/3} \simeq 0.8 \mu\text{m}$, which

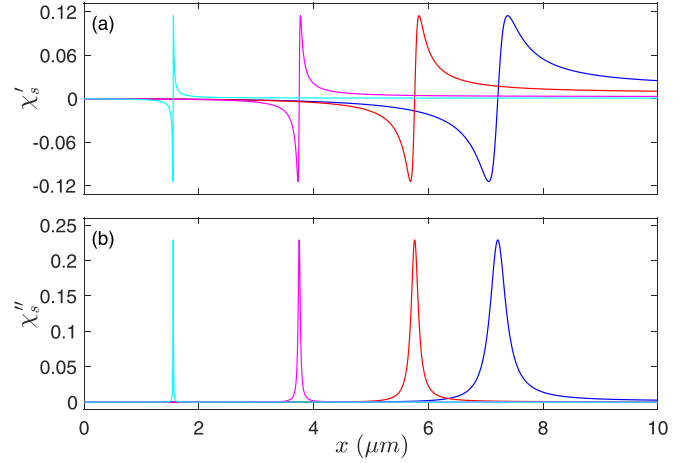


FIG. 2. (a) Real and (b) imaginary parts of signal susceptibility χ_s against position x for a homogeneous sample of target atoms. From left to right, the curves in cyan, magenta, red, and blue refer to $\delta_{\text{eff}}/2\pi = -5.0, -1.2, -0.4,$ and -0.2 MHz, respectively. Other parameters are specified in the first paragraph of Sec. III.

is clearly less than both the vdW distance $d_{\text{vdW}} \simeq 2.4 \mu\text{m}$ and the LeRoy radius $r_{\text{LR}} \simeq 1.1 \mu\text{m}$ [65]. In this case, $\mathcal{V}_3 = C_3/(2d)^3$ can be used to estimate the next-nearest-neighboring interactions while neither $\mathcal{V}_6 = C_6/d^6$ nor $\mathcal{V}_3 = C_3/d^3$ is applicable for the nearest-neighboring interactions [66–68]. Hence, a direct diagonalization of the dipole-dipole molecular Hamiltonian becomes relevant to produce the densely spaced molecular potentials at short interatomic distances [69,70]. With this method we estimate that the dominant nearest-neighboring interactions are at most 10 kHz [65] due to low Rydberg populations ($\rho_{rr}^{\text{max}} \simeq 0.0005$) and thus negligible for $\delta_{\text{eff}}/2\pi \lesssim -100$ kHz of our interest. In addition, effective molecular resonances occurring at different interatomic distances will induce extra loss processes of the effective field Ω_{eff} . The dominant loss rate is proportional to Ω_{eff}^2 and n^{12} [69], with n being the principal quantum number of Rydberg state $|r\rangle$, and becomes negligible ($\ll 1$ kHz) as we choose $|r\rangle \equiv |60S_{1/2}\rangle$ and $\Omega_{\text{eff}}/2\pi = 0.2$ kHz. Note also that the s and p two-atom states will hybridize for $d < d_{\text{vdW}}$, which might lead to antiblockade effects since the symmetric and antisymmetric states have interactions with opposite signs, though this is not an issue here since the interactions are so large compared to other parameters.

For a homogeneous sample of target atoms, we plot in Fig. 2 the dispersion (χ'_s) and absorption (χ''_s) responses against position x by taking a few specific values of effective detuning δ_{eff} in the presence of six control atoms. It is clear that χ'_s and χ''_s exhibit quite narrow spatial profiles and more importantly are out of phase (manifesting as an odd and an even profile, respectively) to a good approximation as δ_{eff} is decreased to be less than -1.2 MHz. It is also clear that the absorption and dispersion profiles tend to be wider in space and become more deviated from their counterparts in the frequency domain as δ_{eff} is increased to be larger than -0.2 MHz. Moreover, we note that the dispersion and absorption profiles may move outside of the atomic sample in the case of $\delta_{\text{eff}} \lesssim -16$ MHz or $\delta_{\text{eff}} \gtrsim -50$ kHz. These findings

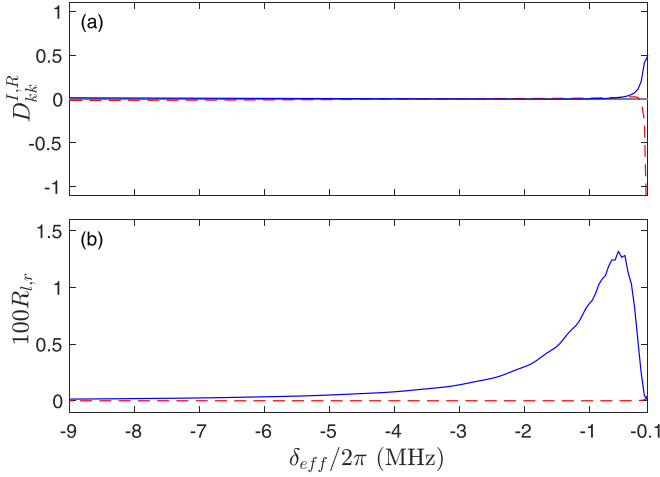


FIG. 3. (a) Figure of merit $D_{kk}^{I,R}$ and (b) reflectivities $R_{l,r}$ against effective detuning δ_{eff} for a homogeneous sample of target atoms with the same parameters as in Fig. 2 except $\lambda_s = 780$ nm. The red-dashed and blue-solid curves refer, respectively, to D_{kk}^R and D_{kk}^I in panel (a) while to R_l and R_r in panel (b).

can be well understood by looking back at Eq. (6), with which it is easy to determine a center $x_c = x_0 + (-C_6/\delta_{\text{eff}})^{1/6}$ where the vdW interactions induce a resonant excitation of relevant target atoms by setting $\delta_{\text{eff}} + \mathcal{V}_6\rho_{33} = 0$ while two half-widths $\delta x_{\pm} = x_0 - x_c + [-C_6/(\delta_{\text{eff}} \mp \gamma_{rg})]^{1/6}$ by setting $\delta_{\text{eff}} + \mathcal{V}_6\rho_{33} = \pm\gamma_{rg}$ with respect to χ'_s and χ''_s in the limit of $\rho_{33} \rightarrow 1$. The nonlinear dependencies of x_c and δx_{\pm} on δ_{eff} answer for why the dispersion and absorption profiles move toward the left side ($x = 0$), become much narrower, and look more symmetric as δ_{eff} is decreased, e.g., from -0.2 to -5 MHz. To be more specific, δx_+ and δx_- will become very different as γ_{rg} is non-negligible as compared to $|\delta_{\text{eff}}|$, so that the profile of χ''_s (χ'_s) is not exactly even (odd) again.

The above results show that χ'_s and χ''_s generally do not vary in phase with the increase or decrease of position x and hence are expected to satisfy the spatial KK relation if both are well contained in the finite atomic sample. The fact is, however, that an essential part of the dispersion and absorption profiles may extend outside of the finite atomic sample when δ_{eff} is either too large or too small, leading to a greater or lesser violation of the spatial KK relation. This has been evaluated by plotting figures of merit $D_{kk}^{I,R}$ in Fig. 3(a), from which we can see that the spatial KK relation is well satisfied with $|D_{kk}^{I,R}| \rightarrow 0$ in a wide range referring to $\delta_{\text{eff}}/2\pi \lesssim -0.2$ MHz, albeit $D_{kk}^I > 0$ and $D_{kk}^R < 0$ turn out to be non-negligible for $\delta_{\text{eff}}/2\pi \gtrsim -0.2$ MHz. Considering that the spatial KK relation is inseparable with unidirectional reflection, we further plot in Fig. 3(b) reflectivities R_l and R_r for a weak signal field incident from the left ($x = 0$) and right ($x = L$) sides, respectively. It shows that unidirectional reflection with $R_l \rightarrow 0$ and $R_r \neq 0$ occurs almost in the whole range of $\delta_{\text{eff}}/2\pi \in [-9.0, -0.1]$ MHz and $R_l \neq 0$ is slightly visible only for $\delta_{\text{eff}}/2\pi \gtrsim -0.2$ MHz where $|D_{kk}^{I,R}|$ increase to be over 0.1, indicating that the spatial KK relation is not strictly required. It is also worth noting that R_r varies with δ_{eff} and becomes maximal at $\delta_{\text{eff}}/2\pi \simeq -0.6$ MHz, in virtue of

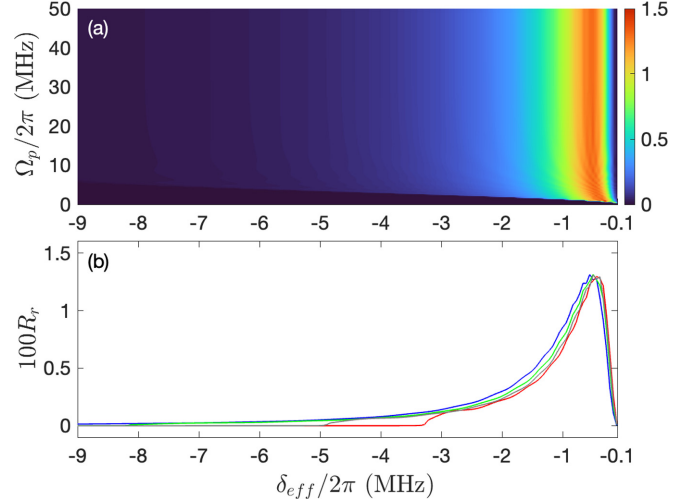


FIG. 4. (a) Reflectivity R , against effective detuning δ_{eff} and Rabi frequency Ω_p for a homogeneous sample of target atoms with the same parameters as in Fig. 3. (b) 1D cuts of 2D plots in panel (a) with $\Omega_p/2\pi = 50, 5.0, 3.0,$ and 2.5 MHz from left to right, respectively.

a trade-off between the degree of spatial KK relation and the width of the real (dispersion) potential χ'_s .

Then we examine two experimental possibilities of modulating unidirectional reflection behaviors based on nonlocal vdW interactions between the control and target Rydberg atoms. One possibility is shown in Fig. 4 where the pumping field Ω_p is used as an experimentally feasible “knob” to control the range of δ_{eff} for observing unidirectional reflection. It is obvious that this range shrinks evidently from the side of smaller δ_{eff} as Ω_p gradually decreases, which refers to $\delta_{\text{eff}} \in [-3.3, -0.1]$ MHz, in particular, for $\Omega_p = 2.5$ MHz. This can be attributed to the fact that a decrease of Ω_p will result in a decrease of ρ_{33} and thus a decrease of x_c for a given δ_{eff} , equivalent to a decrease of the maximal $|\delta_{\text{eff}}|$ referring to $x_c = 0$ and denoting a boundary of the well-satisfied spatial KK relation. The other possibility is shown in Fig. 5 where reflectivity R_r is plotted against Δ_s instead of δ_{eff} , with Δ_c being an alternative control “knob” feasible in experiment. It is easy to see that we can move the range of Δ_s for observing unidirectional reflection as a whole, without shrinking or expanding in terms of both Δ_s and R_r , by modulating Δ_c in the limit of $\Delta_s \simeq -\Delta_c \gg \Omega_c$. This fine-tunability relies on the fact that susceptibility χ_s in Eq. (6) refers to a reduced two-level system where the effective detuning δ_{eff} is mainly contributed by the sum of signal (Δ_s) and coupling (Δ_c) detunings. A reversed unidirectional reflection with $R_l \neq 0$ and $R_r = 0$ requires to excite a second ring of six control atoms at $x = L - x_0$ into the Rydberg state $|3\rangle$ while leaving the first ring of six control atoms at $x = x_0$ free of excitations.

So far we have shown that unidirectional reflection can be realized and modulated for appropriate effective (δ_{eff}) or signal (Δ_s) detunings. However, the nonzero reflectivity $R_r \lesssim 0.013$ is obviously small because both real (χ'_s) and imaginary (χ''_s) potentials are rather weak (i.e., less than unit in magnitudes). In order to enhance χ_s and thus increase R_r , we can choose a larger atomic density N_0 and/or a smaller dephasing rate γ_{rg} as can be seen from Eq. (6). Unfortunately, the former

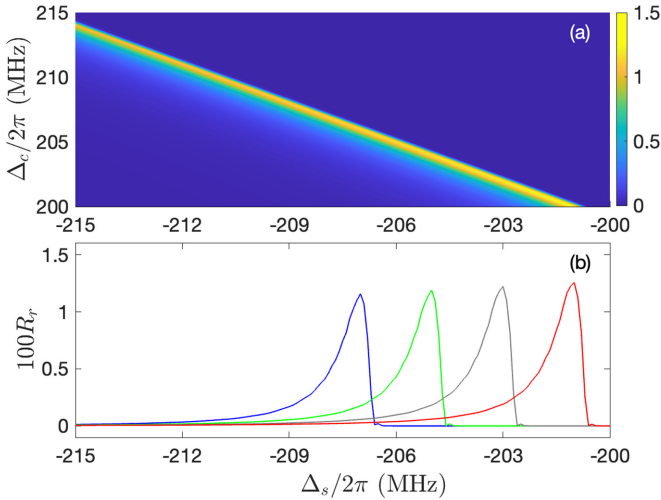


FIG. 5. (a) Reflectivity R_r against signal detuning Δ_s and coupling detuning Δ_c for a homogeneous sample of target atoms with the same parameters as in Fig. 3. (b) 1D cuts of 2D plots in panel (a) with $\Delta_c/2\pi = 206, 204, 202,$ and 200 MHz from left to right, respectively.

choice will invalidate our model described by Eq. (2) in the presence of considerable interactions between target atoms, while the latter choice is restricted by the residual Doppler broadening of cold atoms (e.g., ~ 20 kHz at the temperature of $T = 1 \mu\text{K}$). This motivates us to consider another scenario where the homogeneous atomic sample is replaced by a periodic atomic lattice described by Eq. (12) so as to enhance the nonzero reflectivity by incorporating multiple Bragg scattering into the spatial KK relation.

Two typical examples on periodically modulated dispersion and absorption responses are shown in Fig. 6 with $\delta_{\text{eff}}/2\pi = -0.2$ MHz and $\delta_{\text{eff}}/2\pi = -1.2$ MHz, respectively. Here the lattice period being just a half of the interatomic distance with $d/2 \simeq \Lambda = 400$ nm is appropriate since the

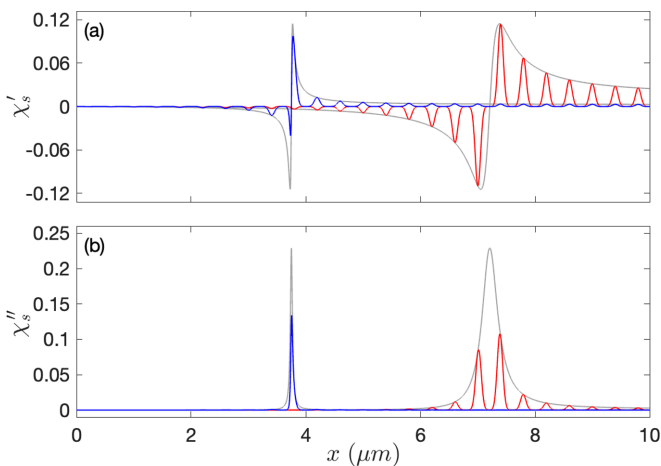


FIG. 6. (a) Real and (b) imaginary parts of signal susceptibility χ_s against position x for a periodic lattice of target atoms with $\delta_{\text{eff}}/2\pi = -1.2$ MHz (left) or -0.2 MHz (right). Relevant parameters are the same as those in Fig. 2 except $\lambda_s = 780$ nm, $\Lambda = 400$ nm, and $\delta x = \Lambda/6$.

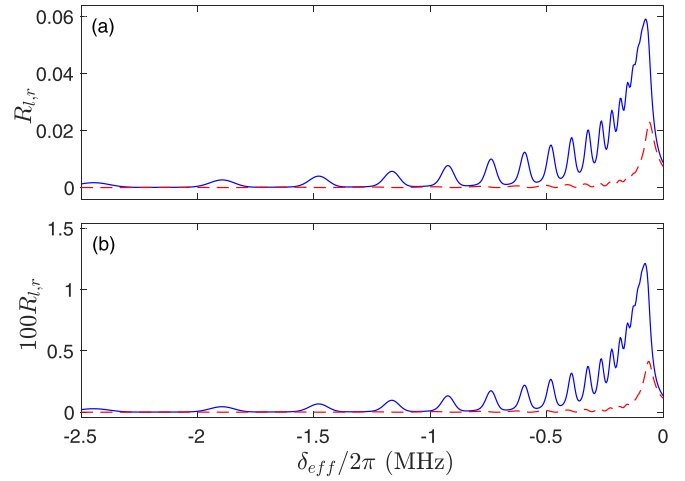


FIG. 7. Reflectivities R_l (red dashed curve) and R_r (blue solid curve) against effective detuning δ_{eff} for a periodic lattice of target atoms with $N_0 = 2.0 \times 10^{12} \text{cm}^{-3}$ (a) or $8.0 \times 10^{11} \text{cm}^{-3}$ (b). Relevant parameters are the same as those in Fig. 2 except $\lambda_s = 780$ nm, $\Lambda = 400$ nm, and $\delta x = \Lambda/6$.

positions of neighboring atoms are different not only in x but also in y and z so that tens of well-separated target atoms can be found in each of the $L/\Lambda = 25$ periods. It is easy to see that χ'_s and χ''_s are out of phase, to different extents depending on δ_{eff} , in their overall profiles similar to their counterparts in Fig. 2. However, it is also obvious that they exhibit comblike fine structures under the not-in-phase overall profiles as a result of the periodic Gaussian density $N(x)$ in Eq. (12). A signal field incident upon the finite atomic lattice is expected to experience an enhanced reflection in the presence of both the spatial KK relation contributed by the overall profiles of χ'_s and χ''_s and the multiple Bragg scattering contributed by the fine structures of χ'_s and χ''_s . This is exactly what we observe in Fig. 7 where unbalanced reflectivities R_l and R_r are plotted against the effective detuning δ_{eff} .

It is easy to see from Fig. 7(a) that one reflectivity is obviously enhanced albeit in an oscillating manner and exhibits the maximum $R_r \rightarrow 0.06$ at $\delta_{\text{eff}} \simeq -75$ kHz, while the other reflectivity remains vanishing only for $\delta_{\text{eff}} \lesssim -200$ kHz and exhibits the maximum $R_l \simeq 0.02$ at $\delta_{\text{eff}} \simeq -60$ kHz. The underlying physics should be that strongest Bragg scattering occurs in the case of $\delta_{\text{eff}} \rightarrow 0$ where χ'_s and χ''_s exhibit very wide but not too low comblike spatial profiles on one hand and tend to vary in phase on the other hand. Figure 7(b) further shows that the asymmetric enhancement of $R_{l,r}$ due to multiple Bragg scattering holds for a smaller density of the periodic atomic lattice with the maximal value $R_r \rightarrow 0.013$ equivalent to that in a homogeneous atomic sample with a larger density [cf. Fig. 3(b)]. These results confirm that multiple Bragg scattering is a valid tool for improving the asymmetric or unidirectional reflection behaviors arising from spatial KK relation. This can be understood by considering that an incident signal field is just reflected once by the unimodal complex potential $\chi_s(x)$ in a homogeneous atomic sample, while it is reflected many times due to Bragg scattering by the comblike fine structures of $\chi_s(x)$ in a periodic atomic lattice with a more or less modified spatial KK relation.

IV. CONCLUSIONS

In summary, we have proposed an efficient scheme for realizing the tunable spatial KK relation by exploiting non-local vdW interactions of Rydberg atoms. Six control atoms in a Rydberg dark state are used to map the dispersion and absorption responses of a homogenous sample or a periodic lattice of target atoms from the frequency domain to the space domain. This is attained as all target atoms are driven in the EIT regime to an effective two-level configuration by a signal and a coupling field kept near resonance on one two-photon transition but far-detuned from two one-photon transitions. Our numerical results show that the spatial dispersion and absorption responses generally do not vary in phase and more importantly could well satisfy the spatial KK relation, hence supporting unidirectional ($R_l = 0$ and $R_r \neq 0$)

reflection behaviors. Note also that periodic atomic lattices seem more appealing than homogenous atomic samples in that they promise an obvious enhancement of the nonzero reflection due to a positive interplay of the multiple Bragg scattering and the spatial KK relation. Our findings should be instructive on combining non-Hermitian quantum optics and coherent manipulation of Rydberg atoms, e.g., to develop one-way optical devices and explore new applications with long-range vdW interactions.

ACKNOWLEDGMENTS

This work is supported by the National Natural Science Foundation of China (Grant No. 12074061) and the National Key Research and Development Program of China (Grant No. 2021YFE0193500).

-
- [1] Z. Lin, H. Ramezani, T. Eichelkraut, T. Kottos, H. Cao, and D. N. Christodoulides, Unidirectional Invisibility Induced by \mathcal{PT} -Symmetric Periodic Structures, *Phys. Rev. Lett.* **106**, 213901 (2011).
- [2] S. Longhi, Invisibility in \mathcal{PT} -symmetric complex crystals, *J. Phys. A: Math. Theor.* **44**, 485302 (2011).
- [3] A. Regensburger, C. Bersch, M.-A. Miri, G. Onishchukov, D. N. Christodoulides, and U. Peschel, Parity-time synthetic photonic lattices, *Nature (London)* **488**, 167 (2012).
- [4] A. Mostafazadeh, Invisibility and \mathcal{PT} symmetry, *Phys. Rev. A* **87**, 012103 (2013).
- [5] L. Feng, Y.-L. Xu, W. S. Fegadolli, M.-H. Lu, J. E. B. Oliveira, V. R. Almeida, Y.-F. Chen, and A. Scherer, Experimental demonstration of a unidirectional reflectionless parity-time metamaterial at optical frequencies, *Nat. Mater.* **12**, 108 (2013).
- [6] G. Castaldi, S. Savoia, V. Galdi, A. Alu, and N. Engheta, \mathcal{PT} Metamaterials via Complex-Coordinate Transformation Optics, *Phys. Rev. Lett.* **110**, 173901 (2013).
- [7] Y. Fu, Y. Xu, and H. Chen, Zero index metamaterials with PT symmetry in a waveguide system, *Opt. Express* **24**, 1648 (2016).
- [8] N. X. A. Rivolta and B. Maes, Side-coupled resonators with parity-time symmetry for broadband unidirectional invisibility, *Phys. Rev. A* **94**, 053854 (2016).
- [9] W. L. Liu, M. Li, R. S. Guzzon, E. J. Norberg, J. S. Parker, M. Z. Lu, L. A. Coldren, and J. P. Yao, An integrated parity-time symmetric wavelength-tunable single-mode microring laser, *Nat. Commun.* **8**, 15389 (2017).
- [10] Y. Huang, Y. Shen, C. Min, S. Fan, and G. Veronis, Unidirectional reflectionless light propagation at exceptional points, *Nanophotonics* **6**, 977 (2017).
- [11] M. Sarisaman, Unidirectional reflectionlessness and invisibility in the TE and TM modes of a \mathcal{PT} -symmetric slab system, *Phys. Rev. A* **95**, 013806 (2017).
- [12] J.-H. Wu, M. Artoni, and G. C. La Rocca, Non-Hermitian Degeneracies and Unidirectional Reflectionless Atomic Lattices, *Phys. Rev. Lett.* **113**, 123004 (2014).
- [13] L. Yuan and Y. Y. Lu, Unidirectional reflectionless transmission for two-dimensional PT-symmetric periodic structures, *Phys. Rev. A* **100**, 053805 (2019).
- [14] S. A. R. Horsley, M. Artoni, and G. C. La Rocca, Spatial Kramers-Kronig relations and the reflection of waves, *Nat. Photonics* **9**, 436 (2015).
- [15] S. Longhi, Bidirectional invisibility in Kramers-Kronig optical media, *Opt. Lett.* **41**, 3727 (2016).
- [16] C. G. King, S. A. R. Horsley, and T. G. Philbin, Zero reflection and transmission in graded index media, *J. Opt.* **19**, 085603 (2017).
- [17] S. A. R. Horsley and S. Longhi, Spatiotemporal deformations of reflectionless potentials, *Phys. Rev. A* **96**, 023841 (2017).
- [18] S. A. R. Horsley and S. Longhi, One-way invisibility in isotropic dielectric optical media, *Am. J. Phys.* **85**, 439 (2017).
- [19] S. Longhi, Kramers-Kronig potentials for the discrete Schrödinger equation, *Phys. Rev. A* **96**, 042106 (2017).
- [20] D. Liu, Y. Huang, H. Hu, L. Liu, D. Gao, L. Ran, D. Ye, and Y. Luo, Designing spatial Kramers-Kronig media using transformation optics, *IEEE Trans. Antennas Propag.* **68**, 2945 (2020).
- [21] W. Jiang, Y. Ma, J. Yuan, G. Yin, W. Wu, and S. He, Deformable broadband metamaterial absorbers engineered with an analytical spatial Kramers-Kronig permittivity profile, *Laser Photonics Rev.* **11**, 1600253 (2017).
- [22] D. Ye, C. Cao, T. Zhou, and J. Huangfu, G. Zheng and L. Ran, Observation of reflectionless absorption due to spatial Kramers-Kronig profile, *Nat. Commun.* **8**, 51 (2017).
- [23] L. Singh, E. D. Epstein, D. Cheskis, S. Sternklar, and Y. Gorodetski, Experimental investigation of Kramers-Kronig relations in chiral metasurfaces with reduced rotational symmetry, *J. Opt.* **22**, 12LT01 (2020).
- [24] Y. Zhang, J.-H. Wu, M. Artoni, and G. C. La Rocca, Controlled unidirectional reflection in cold atoms via the spatial Kramers-Kronig relation, *Opt. Express* **29**, 5890 (2021).
- [25] H. A. Haus, *Waves and Fields in Optoelectronics* (Prentice-Hall, New York, 1984).
- [26] S. Saha, K. V. Sowmya Sai, N. Ghosh, and S. Dutta Gupta, Consequences of nonreciprocity in reflection from a truncated spatial Kramers-Kronig medium, *J. Opt.* **19**, 075401 (2017).
- [27] M. Kulishov, J. M. Laniel, N. Belanger, J. Azana, and D. V. Plant, Nonreciprocal waveguide Bragg gratings, *Opt. Express* **13**, 3068 (2005).

- [28] E. Yang, Y. Lu, Y. Wang, Y. Dai, and P. Wang, Unidirectional reflectionless phenomenon in periodic ternary layered material, *Opt. Express* **24**, 14311 (2016).
- [29] Y. Baek and Y. Park, Intensity-based holographic imaging via space-domain Kramers-Kronig relations, *Nat. Photonics* **15**, 354 (2021).
- [30] C. Lee, Y. Baek, H. Hugonnet, and Y. Park, Single-shot wide-field topography measurement using spectrally multiplexed reflection intensity holography via space-domain Kramers-Kronig relations, *Opt. Lett.* **47**, 1025 (2022).
- [31] Q. Li, Y. Luo, D. Liu, Y. Gao, J. Zhang, L. Ran, and D. Ye, A miniaturized anechoic chamber: Omnidirectional impedance matching based on truncated spatial Kramers-Kronig medium, *Adv. Opt. Mater.* **10**, 2200381 (2022).
- [32] D. Tong, S. M. Farooqi, J. Stanojevic, S. Krishnan, Y. P. Zhang, R. Cote, E. E. Eyler, and P. L. Gould, Local Blockade of Rydberg Excitation in an Ultracold Gas, *Phys. Rev. Lett.* **93**, 063001 (2004).
- [33] T. Vogt, M. Viteau, J. Zhao, A. Chotia, D. Comparat, and P. Pillet, Dipole Blockade at Förster Resonances in High Resolution Laser Excitation of Rydberg States of Cesium Atoms, *Phys. Rev. Lett.* **97**, 083003 (2006).
- [34] T. Baluktsian, B. Huber, R. Low, and T. Pfau, Evidence for Strong van der Waals Type Rydberg-Rydberg Interaction in a Thermal Vapor, *Phys. Rev. Lett.* **110**, 123001 (2013).
- [35] C.-H. Fan, D. Rossini, H.-X. Zhang, J.-H. Wu, M. Artoni, and G. C. La Rocca, Discrete time crystal in a finite chain of Rydberg atoms without disorder, *Phys. Rev. A* **101**, 013417 (2020).
- [36] T. L. Nguyen, Study of dipole-dipole interaction between Rydberg atoms: toward quantum simulation with Rydberg atoms, Doctoral dissertation, Pierre and Marie Curie University, Paris, 2016.
- [37] M. D. Lukin, M. Fleischhauer, R. Cote, L. M. Duan, D. Jaksch, J. I. Cirac, and P. Zoller, Dipole Blockade and Quantum Information Processing in Mesoscopic Atomic Ensembles, *Phys. Rev. Lett.* **87**, 037901 (2001).
- [38] D. Paredes-Barato and C. S. Adams, All-Optical Quantum Information Processing Using Rydberg Gates, *Phys. Rev. Lett.* **112**, 040501 (2014).
- [39] H. Bernien, S. Schwartz, A. Keesling, H. Levine, A. Omran, H. Pichler, S. Choi, S. S. Zibrov, M. Endres, M. Greiner, V. Vuletic, and M. D. Lukin, Probing many-body dynamics on a 51-atom quantum simulator, *Nature (London)* **551**, 579 (2017).
- [40] H. Levine, A. Keesling, A. Omran, H. Bernien, S. Schwartz, A. S. Zibrov, M. Endres, M. Greiner, V. Vuletic, and M. D. Lukin, High-Fidelity Control and Entanglement of Rydberg-Atom Qubits, *Phys. Rev. Lett.* **121**, 123603 (2018).
- [41] N. L. R. Spong, Y. Jiao, O. D. W. Hughes, K. J. Weatherill, I. Lesanovsky, and C. S. Adams, Collectively Encoded Rydberg Qubit, *Phys. Rev. Lett.* **127**, 063604 (2021).
- [42] J. A. Sedlacek, A. Schwettmann, H. Kubler, and J. P. Shaffer, Atom-Based Vector Microwave Electrometry Using Rubidium Rydberg Atoms in a Vapor Cell, *Phys. Rev. Lett.* **111**, 063001 (2013).
- [43] H. Fan, S. Kumar, J. Sedlacek, H. Kubler, S. Karimkashi, and J. P. Shaffer, Atom based RF electric field sensing, *J. Phys. B: At. Mol. Opt. Phys.* **48**, 202001 (2015).
- [44] C. G. Wade, M. Marcuzzi, E. Levi, J. M. Kondo, I. Lesanovsky, C. S. Adams, and K. J. Weatherill, A terahertz-driven non-equilibrium phase transition in a room temperature atomic vapour, *Nat. Commun.* **9**, 3567 (2018).
- [45] K. C. Cox, D. H. Meyer, F. K. Fatemi, and P. D. Kunz, Quantum-Limited Atomic Receiver in the Electrically Small Regime, *Phys. Rev. Lett.* **121**, 110502 (2018).
- [46] M.-Y. Jing, Y. Hu, J. Ma, H. Zhang, L.-J. Zhang, L.-T. Xiao, and S.-T. Jia, Atomic superheterodyne receiver based on microwave-dressed Rydberg spectroscopy, *Nat. Phys.* **16**, 911 (2020).
- [47] M. Saffman and T. G. Walker, Creating single-atom and single-photon sources from entangled atomic ensembles, *Phys. Rev. A* **66**, 065403 (2002).
- [48] T. Peyronel, O. Firstenberg, Q.-Y. Liang, S. Hofferberth, A. V. Gorshkov, T. Pohl, M. D. Lukin, and V. Vuletic, Quantum non-linear optics with single photons enabled by strongly interacting atoms, *Nature (London)* **488**, 57 (2012).
- [49] F. Ripka, H. Kubler, R. Low, and T. Pfau, A room-temperature single-photon source based on strongly interacting Rydberg atoms, *Science* **362**, 446 (2018).
- [50] L. Li and A. Kuzmich, Quantum memory with strong and controllable Rydberg-level interactions, *Nat. Commun.* **7**, 13618 (2016).
- [51] E. Distante, P. Farrera, A. Padron-Brito, D. Paredes-Barato, G. Heinze, and H. de Riedmatten, Storing single photons emitted by a quantum memory on a highly excited Rydberg state, *Nat. Commun.* **8**, 14072 (2017).
- [52] H.-X. Zhang, J.-H. Wu, M. Artoni, and G. C. La Rocca, Single-photon-level light storage with distributed Rydberg excitations in cold atoms, *Front. Phys.* **17**, 22502 (2022).
- [53] H. Gorniaczyk, C. Tresp, J. Schmidt, H. Fedder, and S. Hofferberth, Single-Photon Transistor Mediated by Interstate Rydberg Interactions, *Phys. Rev. Lett.* **113**, 053601 (2014).
- [54] D. Tiarks, S. Baur, K. Schneider, S. Durr, and G. Rempe, Single-Photon Transistor Using a Förster Resonance, *Phys. Rev. Lett.* **113**, 053602 (2014).
- [55] Y.-M. Hao, G.-W. Lin, X.-M. Lin, Y.-P. Liu, and S.-Q. Gong, Single-photon transistor based on cavity electromagnetically induced transparency with Rydberg atomic ensemble, *Sci. Rep.* **9**, 4723 (2019).
- [56] H. R. Gray, R. M. Whitley and C. R. Stroud, Coherent trapping of atomic populations, *Opt. Lett.* **3**, 218 (1978).
- [57] M. O. Scully and M. S. Zubairy, *Quantum Optics* (Cambridge University, Cambridge, England, 1997).
- [58] Y.-Q. Li and M. Xiao, Electromagnetically induced transparency in a three-level Λ -type system in rubidium atoms, *Phys. Rev. A* **51**, R2703(R) (1995).
- [59] Y.-Y. Zou, Y. Jiang, Y.-F. Mei, X.-X. Guo, and S.-W. Du, Quantum Heat Engine Using Electromagnetically Induced Transparency, *Phys. Rev. Lett.* **119**, 050602 (2017).
- [60] L. D. Landau and E. M. Lifshitz, *Electrodynamics of Continuous Media* (Butterworth-Heinemann, Oxford, England, 1984).
- [61] M. Artoni, G. C. La Rocca, and F. Bassani, Resonantly absorbing one-dimensional photonic crystals, *Phys. Rev. E* **72**, 046604 (2005).
- [62] K. Singer, J. Stanojevic, M. Weidemuller, and R. Cote, Long-range interactions between alkali Rydberg atom pairs correlated to the ns - ns , np - np and nd - nd asymptotes, *J. Phys. B: At. Mol. Opt. Phys.* **38**, S295 (2005).
- [63] I. I. Beterov, I. I. Ryabtsev, D. B. Tretyakov, and V. M. Entin, Quasiclassical calculations of blackbody-radiation-induced

- depopulation rates and effective lifetimes of Rydberg nS , nP , and nD alkali-metal atoms with $n \leq 80$, *Phys. Rev. A* **79**, 052504 (2009).
- [64] D. A. Steck, Rubidium 87 D line data, available online at <http://steck.us/alkalidata>.
- [65] N. Šibalić, J. D. Pritchard, C. S. Adams, and K. J. Weatherill, An introduction to Rydberg atoms with ARC, available online at https://arc-alkali-rydberg-calculator.readthedocs.io/en/latest/Rydberg_atoms_a_primer_notebook.html.
- [66] B. Ji, C.-C. Tsai, and W. C. Stwalley, Proposed modification of the criterion for the region of validity of the inverse-power expansion in diatomic long-range potentials, *Chem. Phys. Lett.* **236**, 242 (1995).
- [67] C. Boisseau, I. Simbotin, and R. Cote, Macrodimers: Ultralong Range Rydberg Molecules, *Phys. Rev. Lett.* **88**, 133004 (2002).
- [68] B. Vaucher, S. J. Thwaite, and D. Jaksch, Ultralarge Rydberg dimers in optical lattices, *Phys. Rev. A* **78**, 043415 (2008).
- [69] A. Derevianko, P. Komar, T. Topcu, R. M. Kroeze, and M. D. Lukin, Effects of molecular resonances on Rydberg blockade, *Phys. Rev. A* **92**, 063419 (2015).
- [70] S. Hollerith, K. Srakaew, D. Wei, A. Rubio-Abadal, D. Adler, P. Weckesser, A. Kruckenhauser, V. Walther, R. van Bijnen, J. Rui, C. Gross, I. Bloch, and J. Zeiher, Realizing Distance-Selective Interactions in a Rydberg-Dressed Atom Array, *Phys. Rev. Lett.* **128**, 113602 (2022).